Facies, dissolution seams and stable isotope compositions of the Rohtas Limestone (Vindhyan Supergroup) in the Son valley area, central India

S Banerjee[1], S K Bhattacharya[2] and S Sarkar[3]

[1]*Department of Earth Sciences, Indian Institute of Technology Bombay, Powai, Mumbai 400 076, India.*
e-mail: santanu@iitb.ac.in
[2]*Physical Research Laboratory, Ahmedabad, Navrangpura, Ahmedabad 380 009, India.*
[3]*Department of Geological Sciences, Jadavpur University, Kolkata 700 032, India.*

The early Mesoproterozoic Rohtas Limestone in the Son valley area of central India represents an overall shallowing-upward carbonate succession. Detailed facies analysis of the limestone reveals outer- to inner-shelf deposition in an open marine setting. Wave-ripples, hummocky cross stratifications and edgewise conglomerates argue against a deep marine depositional model for the Rohtas Limestone proposed earlier. Stable isotope analysis of the limestone shows that δ^{13}C and δ^{18}O values are compatible with the early Mesoproterozoic open seawater composition. The ribbon limestone facies in the Rohtas Limestone is characterized by micritic beds, each decoupled in a lower band enriched and an upper band depleted in dissolution seams. Band-wise isotopic analysis reveals systematic short-term variations. Comparative enrichment of the heavier isotopes in the upper bands is attributed to early cementation from sea water and water derived from the lower band undergoing dissolution because of lowering of pH at depth. The short-term positive shifts in isotopic compositions in almost every upward gradational transition from a seamed band to a non-seamed band support the contention that dissolution seams here are of early diagenetic origin, although their formation was accentuated under overburden pressure.

1. Introduction

The Vindhyan sedimentary succession contains unmetamorphosed and mildly deformed carbonates at several stratigraphic levels. There exist several studies on the sedimentary attributes of Vindhyan carbonates, but a process-related facies correlation has not been attempted so far (e.g., Sarkar *et al* 1996; Chakraborty 2004). Even paleogeographic information on the lower Vindhyan carbonates are based on circumstantial evidence and process correlation has been largely ignored leading to occasional controversies. Chatterjee and Sen (1988) considered that lower Vindhyan Rohtas Limestone represents shallow marine deposition whereas Chakraborty *et al* (1996) suggested a deep basinal origin for the same. In some studies, researchers even extrapolated the paleogeography of the Rohtas Limestone based on observations from the upper Vindhyan (Singh 1973; Chanda and Bhattacharyya 1982).

Most of the earlier workers have not considered stable isotope ratios of the carbonates as a supplement to the field and petrographic observations. δ^{13}C and δ^{18}O values of these carbonates may provide significant clues to the Proterozoic history of the earth's climate, atmosphere, hydrosphere and biosphere (Knoll and Swett 1990; Lindsay and Brasier 2000 and many others). A few recent studies have highlighted secular and local changes in stable isotope compositions in Vindhyan carbonates and broad correlation of these changes

Keywords. Dissolution seams; Rohtas Limestone; stable isotopes, diagenesis.

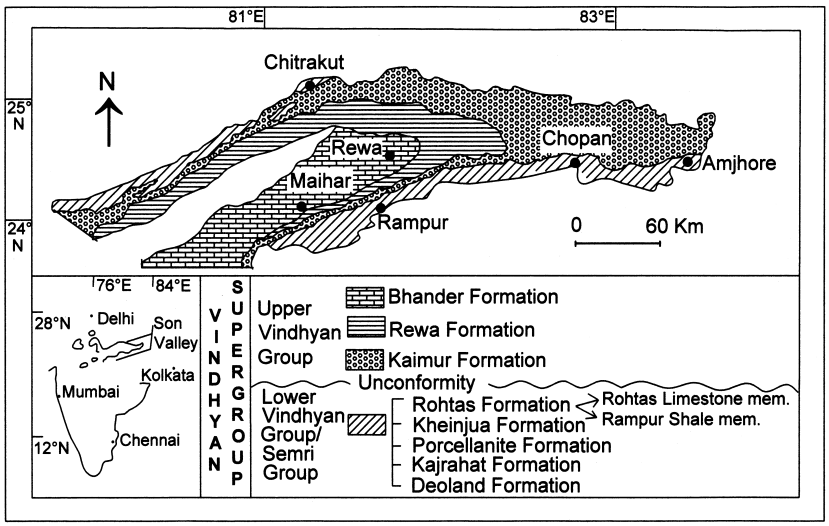

Figure 1. Geological map of the Vindhyan supergroup in the Son valley with location of the study area (modified after Auden 1933) and general stratigraphy of the Vindhyan Supergroup with elaborations in relevant parts (map of India within inset).

with the global isotope evolution curve for marine carbonates has been made (Kumar *et al* 2002; Ray *et al* 2003). An attempt has also been made to locate the Pre-Cambrian/Cambrian boundary within the upper Vindhyan on the basis of isotope variations, although the dataset did not have sufficient resolution for this purpose (Friedman *et al* 1996). It is important to note that short-term variations, of stable isotope compositions may provide a wealth of information about depositional and early diagenetic conditions (Allan and Mathews 1982; Beeunas and Knauth 1985). For example, Chakraborty *et al* (2002) showed that stable isotope data can be facies-sensitive and one should be careful while interpreting secular variations in stable isotope compositions.

An interesting feature of the Rohtas Limestone is the presence of mm- to cm-scale layers enriched and depleted in dissolution seams showing probable evidence of compaction in alternate layers. This feature is not uncommon in carbonate successions of the Phanerozoic or Proterozoic (Byers and Stasco 1978; Bathurst 1987; Bose *et al* 1996) and can arise from differential compaction and cementation. In the case of Rohtas Limestone this feature is intriguing because the alternations do not comply with inferred hydrodynamic changes and instead indicate decoupling of a single bed into multiple layers subsequent to deposition.

Dissolution seams are generally considered to be features of burial diagenesis (Bathurst 1987). However, Bose *et al* (1996) proposed that they can also be pre-burial. Eder (1982) proposed early diagenetic differential cementation involving dissolution of carbonates in the lower layers in a sediment column, subsequent migration of Ca^{2+} and $(CO_3)^{2-}$ ions to the upper layers and reprecipitation there as $CaCO_3$. He thought that dissolution seams develop at a later stage under sediment overburden pressure. Bathurst (1987) objected to Eder's hypothesis based on a mass balance calculation where he found excess Ca^{2+} and $(CO_3)^{2-}$ ion concentrations in the upper layers. Subsequently, Bose *et al* (1996) found dissolution seams within clasts constituting synsedimentary chaotic conglomerates and suggested their generation near the sea floor. None of the workers, however, found any noticeable variation of stable carbon/oxygen isotope ratios between the seamed and non-seamed bands.

This paper presents a detailed process correlation study of the constituent facies of the Rohtas Limestone in the Son valley area near Rampur (figure 1) and discusses their stable isotope characteristics. The purpose is to present an integrated picture based on field studies, petrographic characteristics and stable isotope data in the context of the depositional and diagenetic setting of this Proterozoic carbonate succession. Comparative isotopic studies of the seamed- and non-seamed bands were undertaken to probe the origin of dissolution seams.

2. Geological background

The Vindhyan succession is about 4500 m thick, contains unmetamorphosed beds of sediments which are only mildly deformed, and also contains superbly preserved sedimentary structures both in siliciclastics and carbonates. Earlier works proved that Vindhyan sedimentation took place in an intracratonic setting and is dominantly shallow

marine in nature (Chanda and Bhattacharyya 1982; Bose *et al* 2001).

The Rohtas Formation belongs to the Semri Group, the lower rung of the two-tiered Vindhyan Supergroup (figure 1; Banerjee 1997; Bose *et al* 2001; Rasmussen *et al* 2002) and is exposed along the southern flank of the Vindhyan basin in the Son valley area. In the Rampur area, the grey-to-dark coloured Rampur Shale constitutes the lower member of the Rohtas Formation that overlies the predominantly siliciclastic Kheinjua Formation (figure 1, Banerjee 1997). The Rampur Shale passes upward gradationally into the Rohtas Limestone, which is terminated at the top by an unconformity defining the contact between the Lower Vindhyan and Upper Vindhyan (Bose *et al* 2001). Ray *et al* (2003) claimed a long hiatus between the Lower Vindhyan and the Upper Vindhyan. The pyroclastics occurring in the basal part of the Rampur Shale have been dated recently to 1.6 Ga by the U/Pb SHRIMP technique (Rasmussen *et al* 2002; see also Ray *et al* 2002, 2003). Recently, Sarangi *et al* (2004) dated the carbonaceous fossils (*Grypania*) of the Rohtas Formation with the Pb/Pb dating technique and also obtained an approximate age of 1.6 Ga for the Formation.

3. Facies analysis of Rohtas Limestone

The Rohtas Limestone in the Rampur area consists of six distinct facies occurring repeatedly. Brief description and process interpretation of these facies are given below.

3.1 *Facies A: Black shale*

The lower part of the Rohtas Limestone succession in the Rampur area contains even-bedded fissile, carbonaceous black shale and micritic limestone (figure 2) having a maximum thickness of about 65 cm. Organic carbon content in the shales is on the average 1.8% (Banerjee 1997). Circular black discoidal bodies (up to 0.8 cm diameter) identified as *Chuaria circularis* are occasionally present within the shales. Under the microscope, the shale shows wavy and crinkly laminae (figure 3) containing sparsely distributed quartz silts.

The dark colour of the shales, their high organic carbon content and complete lack of current structure suggests calm and quiet anoxic depositional conditions in an outer shelf setting. Wavy and carbonaceous laminae within the shale strongly suggest microbial mat origin (Schieber 1999; Banerjee and Schieber 2003). Quartz silts within the black shales suggest trapping and binding action of microbial mat. Precambrian black shales differ from Phanerozoic black shales in that

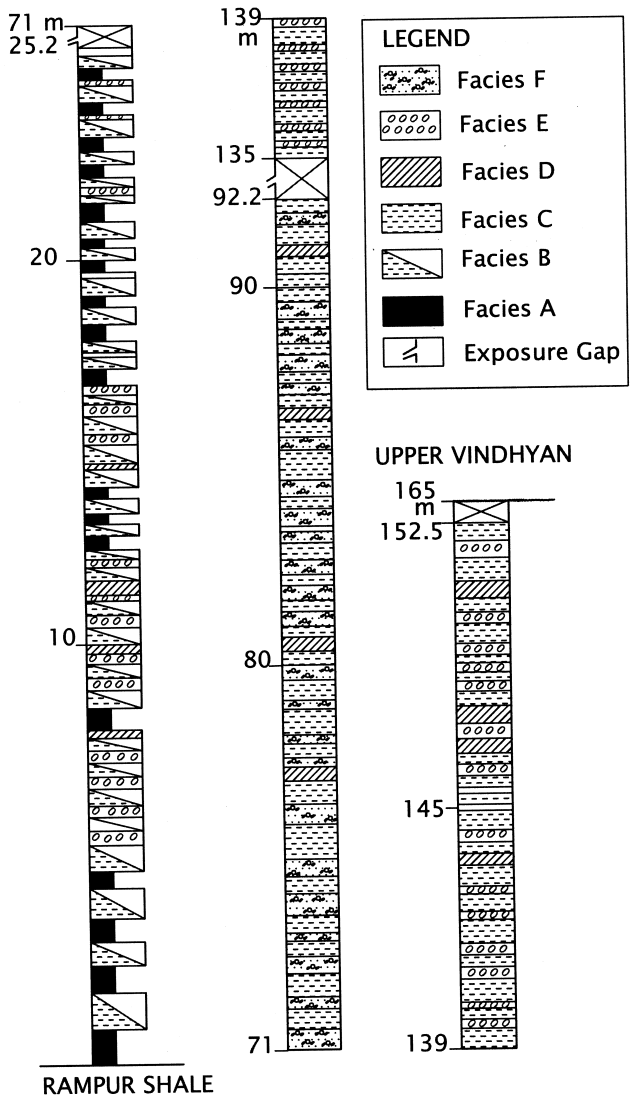

Figure 2. Facies log of the Rohtas Limestone in the Rampur area bounded by the Rampur shale below and the Upper Vindhyan Group above. The contact between the Rampur shale and Rohtas Limestone is gradational. The latter maintains unconformable contact with the upper Vindhyan group.

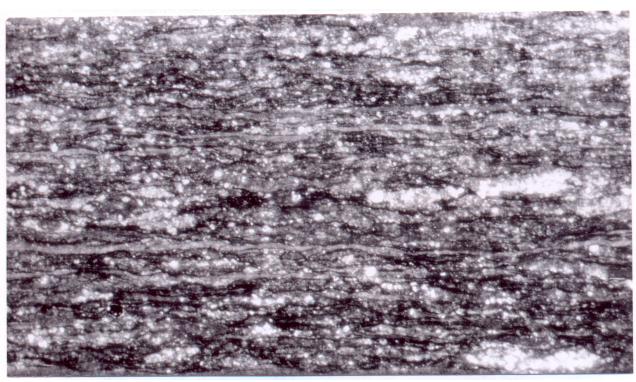

Figure 3. Photomicrograph showing wavy and crinkle laminations within the black shale. Note that quartz grains are sprinkled throughout the section (plane polarized light, long dimension of the photograph = 4.85 mm).

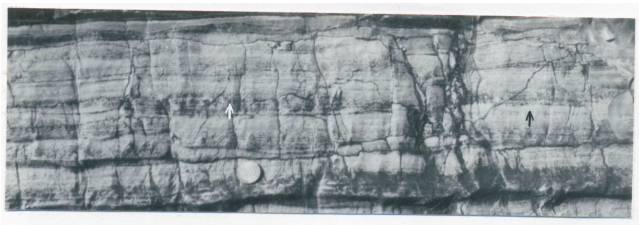

Figure 4. Alternate seamed (white arrow) and non-seamed (black arrow) bands in the Rohtas Limestone. Note the gradational contact between seamed- to the non-seamed bands (coin diameter = 2.6 cm).

the latter were formed in a deep basinal euxinic environment, but the former represent deposition in a subtidal setting (Schieber 1999).

3.2 *Facies B: Ribbon limestone*

Laterally persistent alternating dark and white calcimicrite bands of average thickness 2.5 cm characterize this facies whose average thickness is about 60 cm (figure 4). This facies is also confined to the basal part of the Rohtas Limestone and alternates with facies A. The darker bands contain numerous coalescing or near-coalescing dissolution seams of length varying from 1 mm to 4.5 cm. The white bands are devoid of seams except at their base, which is gradational. The frequency of occurrence of dissolution seams within the seamed bands decreases upward towards the gradational contact with the superjacent non-seamed bands. Base of the seamed band is, however, invariably sharp. The darker bands are argillaceous as suggested by the concentration of insoluble residue along dissolution seams. The seamed bands, in all the couplets, are noticeably enriched in organic carbon (table 1). Both the bands contain minute quartz crystals and non-ferroan dolorhombs, though not in significant amounts.

Smooth lamination, absence of current structures and presence of rare terrigenous particles of minute size indicate deposition beneath the wave base. Each couplet comprising a seamed band and the immediately overlying non-seamed band, with a gradational contact between them, represents the product of a single sedimentation phase. The beds appear to have decoupled into a lower compacted part and an upper uncompacted part. Presumably the lower part remained uncemented when the compaction took place.

3.3 *Facies C: Thin bedded limestone*

Thin-bedded impure calcisiltite is a dominant constituent of the upper part of the succession. The bedding is typically wavy with internal ripple laminae. Fossilized ripples on bed top are symmetric

Table 1. *Stable isotopic ratios of seamed- and non-seamed band couplets taken from facies B at different stratigraphic levels and corresponding organic carbon contents.*

Sample no.	Description	Distance from base of Rohtas Limestone (m)	$\delta^{13}C$ (‰)*	$\delta^{18}O$ (‰)*	Organic carbon (%)
RI-20	Non-seamed	23	−0.6	−5.2	0.12
RI-19	Seamed		−1.3	−6.8	0.35
RI-18	Non-seamed	21	−0.6	−5.2	0.11
RI-17	Seamed		−1.0	−6.0	0.32
RI-16	Non-seamed	20	−0.5	−5.7	0.20
RI-15	Seamed		−1.2	−6.5	0.58
RI-14	Non-seamed	18	−0.3	−6.1	0.15
RI-13	Seamed		−0.7	−7.2	0.40
RI-12	Non-seamed	15	−0.3	−5.8	0.15
RI-11	Seamed		−0.6	−7.1	0.45
RI-10	Non-seamed	12	−0.5	−5.8	0.12
RI-9	Seamed		−0.9	−6.7	0.45
RI-8	Non-seamed	8.5	−1.5	−5.6	0.20
RI-7	Seamed		−1.3	−7.6	0.45
RI-6	Non-seamed	6	−0.7	−5.7	0.12
RI-5	Seamed		−1.5	−7.2	0.45
RI-4	Non-seamed	3.5	−0.5	−6.3	0.11
RI-3	Seamed		−1.4	−7.7	0.45
RI-2	Non-seamed	2	−0.6	−5.5	0.18
RI-1	Seamed		−1.2	−7.3	0.4

*Relative to PDB.

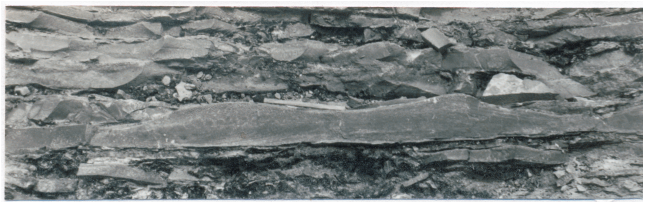

Figure 5. Fossilized ripples (centre) in the facies C (match-stick length = 4.5 cm).

Figure 6. Hummocks and swells in facies D (match-stick length = 4.5 cm).

Figure 7. Climbing ripple set gradationally overlying plane laminations in facies D (match-stick length = 4.5 cm).

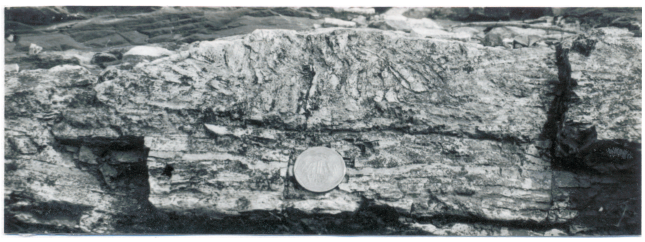

Figure 8. Edgewise conglomerates. Note upright fan-like structure at the middle giving way laterally to bed-parallel clast arrangement in facies D (coin diameter = 2.6 cm).

to near-symmetric in profile (figure 5) with straight or slightly sinuous crests and locally show bi-directional cross laminae. The ripples have an average wavelength of 7 cm and amplitude of 1.5 cm. The ripple crests are oriented NNW–SSE. Facies unit thickness is up to 1.3 m.

This facies was evidently deposited at a shallower depth than facies B. Based on the nature of ripples we infer that deposition occurred above the fair weather wave base.

3.4 *Facies D: Calcarenite*

This calcarenite facies forms tabular beds of average thickness $\sim$ 25 cm disrupting the fine-grained motif of both facies B and C. The beds have occasional basal clast concentrations. Internally, they show tabular and down-slope wedging cross stratifications. Hummocky cross stratifications (De Raaf *et al* 1977) overlying planar laminae are also present (figure 6). The amplitude and wavelengths of the hummocks are, on average, 8.5 cm and 21 cm respectively. Climbing ripples locally occur above the planar laminae (figure 7). Starved ripples on the bed surfaces have about 4.5 cm wavelength and 1.2 cm amplitude. The contact between the sets of plane laminae and ripple laminae appears to be gradational. Unidirectional cross-strata indicate northwesterly paleocurrent direction.

The calcarenite facies encased within thick units of calcimicrite (facies B) and calcisiltite (facies C) seems to have been laid down by episodic storm-originated wave-cum-current combined flow (Dott and Bourgeois 1982, Sarkar *et al* 1996). The basal clast concentration, planar laminae passing up into either small hummocks or wave ripples clearly indicate a waning nature of the flows from which deposition took place.

3.5 *Facies E: Flake-conglomerate*

This facies shows flake-like carbonate intraclasts, similar to those described by Tucker (1982) and Sepkoski (1982). Maximum clast length is about 18 cm, while maximum thickness is only about 2.2 cm. This facies occurs more commonly in the lower part of the Rohtas Limestone and in close association with facies B. In the upper part, when they occur, they are associated with facies C. Thinner beds are broadly lenticular, whereas beds thicker than about 20 cm show strong lenticular geometry with flat bases and irregular convex upward tops. The most striking aspect of the thick beds is edgewise clast fabric in chaotic as well as fan shaped arrangement (figure 8). Steeply inclined clasts, often stacked up in clusters, laterally give way to gently inclined clast assemblages. Some clasts are lodged between two subvertical clasts. Though poorly sorted, the clast composition is uniform and similar to that of the substratum. Interestingly, in many beds there are distinct linings of dark calcite cement selectively at the undersurface of the clasts. Excellent drusy growth characterizes the cement (figure 9). Crystals constituting the clasts have often undergone aggrading

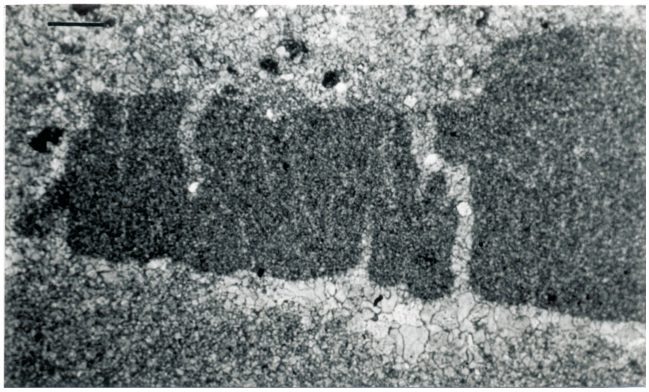

Figure 9. Photomicrograph of a dark clast with incipient or fully grown transverse cracks. Note cement crystals exhibiting drusy growth under the clasts (polarized light, long dimension of the photograph = 1.8 mm).

Figure 10. Conglomerate showing chaotic arrangement of clasts (coin diameter = 2.6 cm).

neomorphism, the constituent crystals being dirty and their mutual boundaries sutured.

These edgewise conglomerates have a striking similarity with those reported from high-energy beaches and tidal bars (Dionne 1971; Ball 1976) but it is clear that they formed in a subtidal mud-depositing environment where clusters of sub-vertical clasts in the beds indicate deposition from laminar sediment gravity flows (Enos 1977). The framework-supported nature of these conglomerates, their edgewise internal fabric, uniformity in clast composition, lack of grading and large size of the clasts argue against deposition from turbidity current. Encasement of these conglomerates within muddy sediments clearly reveals deposition from episodic flow events.

Li and Komar (1986) have noted that the threshold movement of elongate gravel in light density flows usually consists of sliding rather than pivoting. But sliding can give rise to only low inclination of the intraclasts, with imbrications dominating where current velocities are high. The turning force necessary to cause rotations of plate-like intraclasts comes from competing forces of fluid drag and interactions between the intraclasts and the bed or other intraclasts (Allen 1982). If bed shear stress is sufficient, intraclasts can rotate around them. The steeply inclined clasts giving rise to fan-like structures and clasts inserted between subvertical clasts indicate that pivoting must have occurred during transport.

Interaction between the orbital motions of storm waves and the coastal downwelling associated with wind-generated hydrostatic pressure gradients produces the most intense boundary shear stresses on the shelves (Sneeden *et al* 1988). Strongly erosive storm-driven combined flow is the most likely agent to produce the edgewise conglomerate beds in the marine Rohtas Limestone (Mount and Kidder 1993). The geopetal cement under the clasts suggests vadose diagenesis.

3.6 *Facies F: Non-edgewise conglomerate*

Clasts within the facies F are commonly chaotic in arrangement and ungraded showing no significant elongation (figure 10). The conglomerates have laterally variable thickness (maximum ~ 60 cm). There is discernible reverse grading (thickness up to 25 cm) restricted to the lower part of the beds, while the upper parts are normally graded or massive. They may be clast- or matrix-supported. In some beds, clasts are chaotically oriented and some protrude above the bed surface making it irregular.

Deposition of these conglomerates probably took place from debris flows of high matrix strength or modified grain flows with internal grain friction (Postma *et al* 1988). Strong basal shear and development of dispersive pressure at the flow base is indicated by the basal reverse grading. Upward transition from reverse to normal grading probably records surface transformation of a laminar flow as documented by Hampton (1975).

3.7 *Facies succession*

The presence of wave ripples, hummocky cross-stratification and edgewise conglomerates of storm origin attests to shelf deposition of the Rohtas Limestone (figure 2; Banerjee 1997). The Rohtas Limestone succession gradationally overlies the offshore-originated Rampur Shale. In the lower part, black shales alternate with dissolution seams bearing limestone bands, both lacking current features. Upwards, the black shales are replaced by edgewise conglomerates, wave rippled and cross-stratified limestone implying overall progradation (Highstand Systems Tract, Bose *et al* 2001).

4. Methodology

Spot thickness of the constituent facies was measured from quarries to prepare the representative section of the vertical facies variation within the Rohtas Limestone. Fresh samples were collected while noting their respective facies and stratigraphic position. Isotope analysis of the samples was performed at the Physical Research Laboratory, Ahmedabad. Care was taken to choose visibly unaltered micritic carbonate samples identified from prior petrographic studies involving light microscope and SEM. Samples containing recrystallisation veins, neomorphic calcites and dolomites were not chosen for isotope analysis. Chosen samples were cleaned, disaggregated and then powdered. For taking powdered samples from individual seamed- and non-seamed bands, we used hand drills. Carbon and oxygen isotope ratios were measured by treating the powdered samples with H_3PO_4 at 50°C for 10 minutes, cleaning the evolved CO_2 from water vapour and other condensable gases and analyzing it in a VG Micromass 903 D triple collector mass spectrometer. The isotopic ratios δ^{13}C and δ^{18}O are expressed with respect to the international standard PDB (Craig 1957) and are reproducible to ± 0.10‰ at 1σ level. Organic carbon content of the same powdered samples was measured following Dean's (1974) method.

5. General isotopic character of the Rohtas Limestone

Isotopic analysis was done on 31 carbonate samples of which 20 samples belonged to 10 couplets of seamed and non-seamed bands of facies B. The remaining 11 samples are from other constituent facies. δ^{13}C values of Rohtas Limestone samples range from -0.3 to -1.5‰ whereas δ^{18}O values range from -5.2 to -8.7‰ (tables 1 and 2; figure 11). The δ^{13}C values are compatible with normal shallow marine carbonate deposits of early Mesoproterozoic age (Knoll and Swett 1990; Hall and Veizer 1996; Lindsay and Brasier 2000; Shields and Veizer 2002; Kumar *et al* 2002; Ray *et al* 2003). In most of the Mesoproterozoic limestones, δ^{13}C values are close to zero per mil unlike Paleoproterozoic and Neoproterozoic samples which show appreciable δ^{13}C variations (Kaufman and Knoll 1995; Hoffman *et al* 1998; Ray *et al* 2003). δ^{18}O values also agree well with the expected range of unaltered Mesoproterozoic samples (Burdett *et al*

Table 2. *Stable carbon and oxygen isotope compositions of samples from Rohtas Limestone for facies other than facies B from different stratigraphic levels.*

Sample no.	Facies	Distance from base of Rohtas Limestone (m)	δ^{13}C (‰)*	δ^{18}O (‰)*
RI-31	C	152	−1.3	−5.7
RI-30	E	151	−1.4	−8.7
RI-29	D	149	−1.5	−6.9
RI-28	D	147	−1.1	−7.0
RI-27	D	143	−1.2	−7.1
RI-26	E	140	−1.3	−7.2
RI-25	F	90	−1.4	−7.4
RI-24	C	85	−1.3	−6.5
RI-23	C	72	−1.1	−7.3
RI-22	E	15.5	−1.0	−5.8
RI-21	E	5.6	−0.9	−6.0

*Relative to PDB.

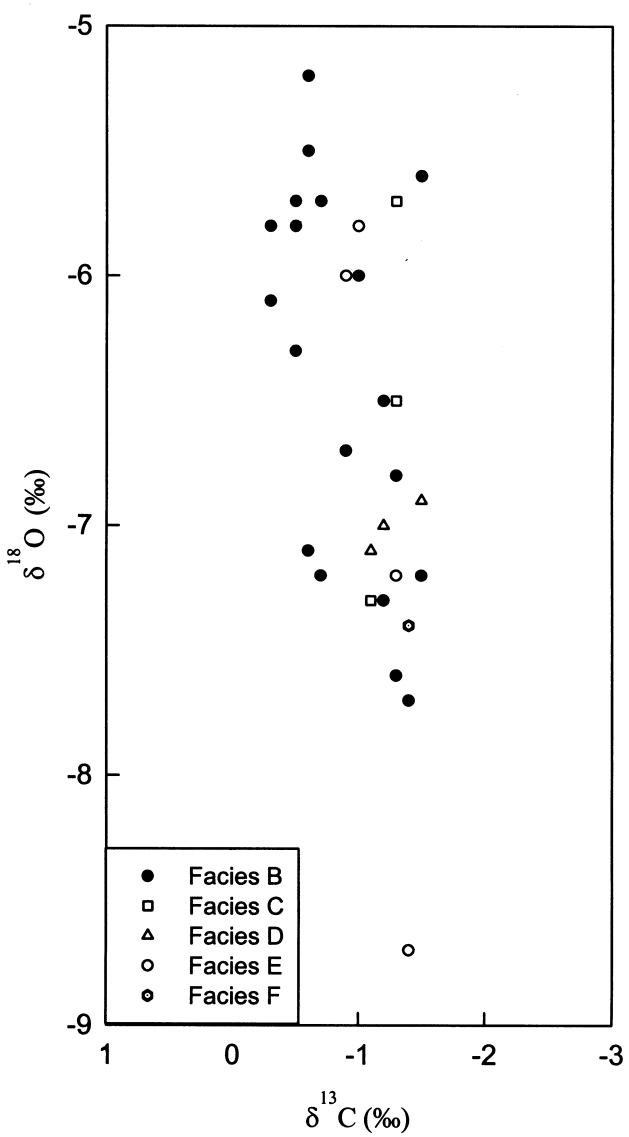

Figure 11. Cross-plot of δ^{13}C and δ^{18}O ratios of all the facies comprising the Rohtas Limestone. For values see tables 1 and 2 . Note that the isotopic compositions do not have any significant correlation denoting absence of major diagensis.

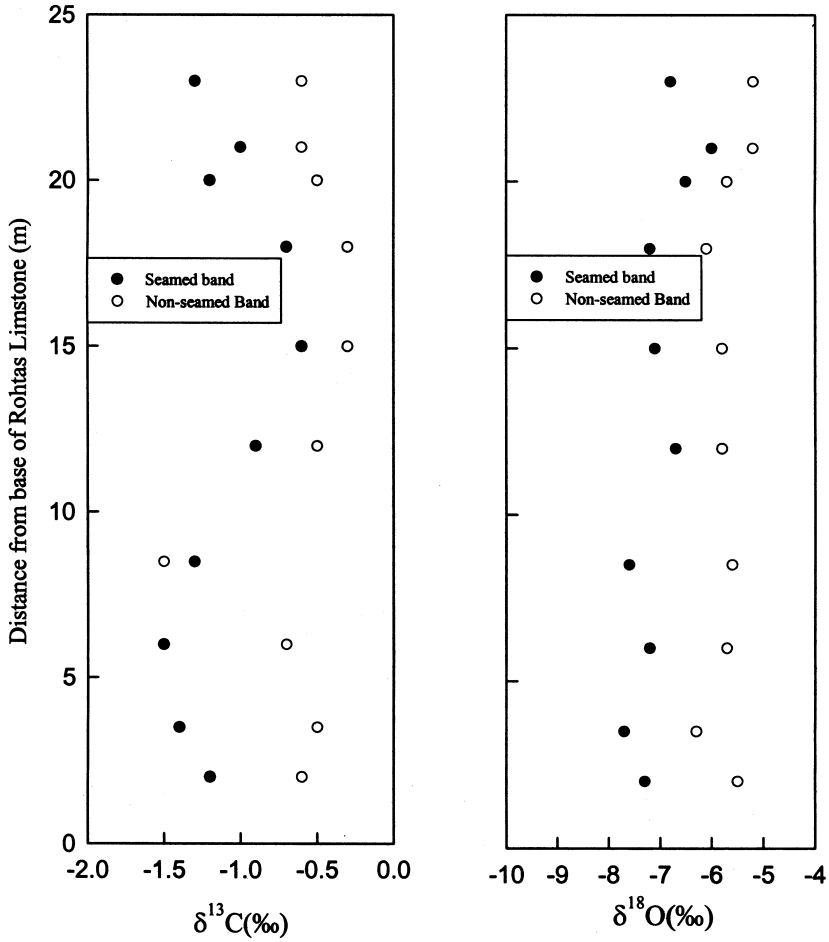

Figure 12. δ^{13}C and δ^{18}O ratios of 10 pairs of seamed- and non-seamed bands from different stratigraphic levels. Note that δ^{13}C and δ^{18}O values of the non-seamed bands are always slightly higher in the pairs except for δ^{13}C in one case (fourth from bottom). The systematic difference is believed to be due to the effect of cementation and dissolution in the band pair during early diagenesis on the sea floor.

1990; Shields and Veizer 2002; Ray *et al* 2003). The restricted range of δ^{13}C and δ^{18}O values corroborates the view that our samples are not significantly altered by diagenetic processes. A good number of samples from the Rohtas Limestone have also been analyzed recently by Kumar *et al* (2002) and Ray *et al* (2003). Based on the combined database, one can safely infer that post-depositional alteration of the present sample set is insignificant. A cross-plot of δ^{13}C and δ^{18}O values does not show any significant correlation to indicate diagenetic alteration (figure 11).

6. Systematic isotopic variations within the Ribbon Limestone

δ^{13}C and δ^{18}O ratios of 10 couplets taken from the seamed and non-seamed bands in facies B have been measured across a vertical succession and are given in table 2 and shown in figure 12 as a function of height. The ratios show a systematic pattern of variation when plotted this way. Every upward transition from a seamed lamina to its overlying non-seamed lamina is associated with enrichment in heavy carbon and oxygen isotopes. Within each couplet, non-seamed bands are invariably richer in ^{18}O by 0.7‰ to 2.1‰ (average 1.2‰). The same trend is also recorded in ^{13}C except for one pair (fourth from bottom in figure 12). In the case of ^{13}C the non-seamed band is richer by 0.3‰ to 1.0‰ (average 0.6‰). The shifts are minor in magnitude, but significant in their systematic recurrence and unidirectional nature.

Such cyclic shifts on mm-scale cannot be explained by ocean water turnover (Aharon and Liew 1992), changes in burial rate of organic carbon (Knoll *et al* 1986, Schidlowski 2001) or meteoric water influx (Allan and Mathews 1982). Evaporative fractionation may cause enrichment in heavy isotopes in non-seamed bands, but salinity variation in such rapid pulsation within an open marine depositional setting is unlikely. We propose that

the observed changes in isotope ratios are related to differential cementation that also decouple the beds in seamed- and non-seamed bands.

Decoupling of beds in compacted (lower) and uncompacted (upper) bands strongly suggests early, pre-compaction differential cementation of the upper bands. Additionally, the systematic variation in isotope ratios between the two types of bands suggests a change in character of the ambient water involved in the process. This observation is consistent with the hypothesis of Bose *et al* (1996) that proposes bed decoupling on the sea floor. They also proposed derivation of the early cement within the upper layer not only from the immediately underlying layer (subjected to dissolution), but also from sea water. Inorganic carbonate cement being richer in heavier isotopes (Hudson, 1977) addition of such cement in the non-seamed band can account for the observed enrichment. As a further support, Hudson (1977) also shows that shallow marine cements are richer in ^{18}O than most other lime components. Significant addition of ions from sea water further accounts for the discrepancy in Bathurst's (1987) mass balance calculation.

7. Conclusions

Deposition of the Mesoproterozoic Rohtas Limestone in central India took place on a storm-dominated open marine shelf extending beneath the storm wave base. Stable carbon and oxygen isotope ratios of the various constituent facies of the formation are consistent with average Mesoproterozoic shallow marine limestone and reflect little facies-specific changes in compliance with overall progradational trend of the succession.

Regular short-term variations in the stable isotope ratios are found in beds with a lower band enriched in dissolution seams relative to the adjoining upper band (depleted in seams). Positive shift in the ratios in vertical gradational transition from the lower to the upper band reflects early diagenetic origin of the dissolution seams. We propose that dissolution of carbonate beneath the seafloor due to lowering of pH followed by cement precipitation at the surface caused the decoupling of beds in such band pairs.

Acknowledgements

SB is thankful to the Department of Science and Technology for financial support and to the Department of Earth Sciences, IIT Bombay for infrastructural support. S S is thankful to Jadavpur University for infrastructural support. The authors thank R A Jani for assistance in analytical work, and Jyotiranjan S Ray and P K Bose for critical reviews and comments on an earlier version of the manuscript.

References

Aharon P and Liew T C 1992 An assessment of the Precambrian/Cambrian transition events on the basis of carbonate isotope record. In: Early Organic Evolution: Implications for Minerals and Energy Resources (eds) M Schidlowski, S Golubic, M M Kimberley, D M Mc Kirdy and P A Trudinge (Berlin: Springer-Verlag), Pp. 211–223.

Allan J R and Mathews R K 1982 Isotope signatures associated with early meteoric Diagenesis; *Sedimentology* **29** 797–817.

Allen J R L 1982 Sedimentary structure, their characters and physical basis. Vol. II. Developments in Geology, Chap 30 B (Amsterdam: Elsevier), Pp. 663.

Auden J B 1933 Vindhyan sedimentation in Son valley; *Geol. Surv. Ind. Mem.* **62** 141–150.

Ball D F 1976 Close-packed patterned arrangements of stones and shells on shore-line Platforms; *Biul. Peryglac.* **25** 5–7.

Banerjee S 1997 Facets of the Mesoproterozoic Semri Sedimentation in Son valley, India. Unpubl. Ph.D. thesis, Jadavpur University, Kolkata, p. 137.

Banerjee S and Schieber J 2003 Paleoproterozoic condensed zone sediments in the Kajrahat Formation, Vindhyan Supergroup, central India; Geological Society of America Abstracts with programs, November 2–5, Seattle, **35**, Abstract No. 64226.

Bathurst R G C 1987 Diagenetically enhanced bedding in argillaceous platform limestones: stratified cementation and selective compaction; *Sedimentology* **34** 749–778.

Beeunas M A and Kanuth L P 1985 Preserved stable isotope signature of subaerial diagenesis in the 1.2 b.y. Mescal Limestone, central Arizona: implication for the timing and development of a terrestrial land plant cover; *Geol. Soc. Am. Bull.* **96** 737–745.

Bose P K, Sarkar S and Bhattacharya S K 1996 Dissolution seams: some observations from the Proterozoic Chanda Limestone, Adilabad, India; Carbonates sand Evaporites **11** 70–76.

Bose P K, Sarkar S, Chakraborty S and Banerjee S 2001 Overview of the Meso- to Neoproterozoic evolution of the Vindhyan basin, central India; *Sed. Geol.* **141** 395–419.

Burdett J W, Grotzinger J P and Arthur M A 1990 Did major changes in Proterozoic seawater occur? *Geology* **18** 227–230.

Byers C W and Stasco L E 1978 Trace fossils and sedimentologic interpretations – Mc Gregor Member of Plateville Formation (Ordovician) of Wisconsin; *J. Sed. Pet.* **48** 1303–1309.

Chakraborty P P, Sarkar A, Bhattacharyya S K and Sanyal P 2002 Isotopic and sedimentologic clues to productivity changes in the Late Riphean sea: a case study of two intracracratonic basins of India; *Proc. Indian Acad. Sci. (Earth Planet. Sci.)* **111(4)** 379–370.

Chakraborty P P 2004 Facies architecture and sequence development in a Neoproterozoic carbonate ramp: Lakheri Limestone Member, Vindhyan Supergroup, Central India; *Precamb. Res.* **132** 29–53.

Chakraborty T, Sarkar S, Chaudhary A K and Das Gupta S 1996 Depositional environment of Vindhyan and other Purana basins: a reappraisal in the light of recent findings. In: Recent Advances in Vindhyan Geology (ed.) Bhattacharyya A, *Mem. Geol. Soc. Ind.* **36** 101–126.

Chanda S K and Bhattacharyya A 1982 Vindhyan sedimentation and paleogeography: post-Auden developments. In: Geology of Vindhyanchal (eds) K S Valdiya, S B Bhatia and V K Gaur (Hindusthan Publishing Corporation: Delhi), Pp. 88–101.

Chatterjee B K and Sen P K 1988 Spectral analysis of a Precambrian limestone-shale sequence, Lower Vindhyan, India; *Precamb. Res.* **39** 139–149.

Craig H 1957 Isotopic standards for each carbon and oxygen correlation factors for mass spectrometric analysis of carbon dioxide; *Geochim. Cosmochim. Acta* **12** 133–149.

Dean W E 1974 Determination of carbonate and organic matter in calcareous sediments and sedimentary rocks by loss on ignition: comparison with other methods; *J. Sed. Pet.* **44** 242–248.

De Raaf J F M, Boersma J R and Vangelder A 1977 Wave-generated structures and sequences from a hallow marine succession, Lower carboniferous County Cork, Ireland; *Sedimentology* **24** 451–483.

Dionne J 1971 Vertical packing of flat stones; *Can. J. Earth Sci.* **8** 1585–1591.

Dott R H Jr And Bourgeois J 1982 Hummocky cross stratification: significance of its variable bedding sequences; *Bull. Geol. Soc. Am.* **93** 663–680.

Eder F W 1982 Diagenetic redistribution of carbonate, a process in forming marl-limestone alternations (Devonian and Carboniferous), Rhenisches Schiefergebrige, W. Germany. In: Cyclic and Event Stratification (eds) G Einsele and A Seilacher (Berlin: Springer-Verlag), Pp. 93–124.

Enos P 1977 Tamabra Limestone of the Poza Rica Trend, Cretaceous, Mexico; *Special Publ. Soc. Econ. Paleont. Miner.* **25** 273–314.

Friedman G M, Chakraborty C and Kolkas M M 1996 Excursion in the end-Proterozoic strata of the Vindhyan basin (central India): its chronostratigraphic significance; Carbonates and evaporites **11** 206–212.

Hall S M and Veizer J 1996 Geochemistry of Precambrian carbonates.VII. Belt Supergroup, Montana and Idaho, U.S.A; *Geochim. et Cosmochim. Acta* **60** 667–977.

Hampton M A 1975 Competence of fine grained debris flows; *J. Sed. Pet.* **45** 834–844.

Hoffman P F, Kaufman A J, Halverson G P and Schrag D P 1998 A Neoproterozoic snowball earth; *Science* **281** 1342–1346.

Hudson J D 1977 Stable isotopes and limestone lithification; *J. Geol. Soc. London* **133** 637–660.

Kaufman A J and Knoll A H 1995 Neoproterozoic variations in the C-isotopic compositions of the seawater: stratigraphic and biogeochemical implications; *Precamb. Res.* **73** 27–49.

Knoll A H, Hayes J M, Kaufman A J, Swett K and Lambert I B 1986 Secular variations in carbon isotope ratios from Upper Proterozoic successions of Svalbard and East Greenland; *Nature* **321** 832–838.

Knoll A H and Swett K 1990 Carbonate deposition during the late Proterozoic era: an example from the Spitsbergen; *Am. J. Sci.* **290A** 104–132.

Kumar B, Das Sharma S, Sreenivas B, Dayal A M, Rao M N, Dubey N and Chawla B R 2002 carbon, oxygen and strontium isotope geochemistry of Proterozoic carbonate rocks of the Vindhyan basin, central India. *Precamb. Res.* **113** 43–63.

Li Z and Komar P D 1986 laboratory measurements of pivoting angles for applications to selective entrainment of gravel in a current; *Sedimentology* **33** 413–423.

Lindsay J F and Brasier M D 2000 A carbon isotope reference curve for 1700–1575 Ma, Mc Arthur and Mt Isa Basins, northern Australia. *Precamb. Res.* **99** 271–308.

Mount J F and Kidder D L 1993 Combined flow origin of edgewise intraclast conglomerates: Sellick Hill Formation (Lower Cambrian), South Australia; *Sedimentology* **40** 315–329.

Postma G, Nemec W and Kleinspehn K L 1988 Large floating clasts in turbidites, a mechanism for their emplacement; *Sedi. Geol.* **58** 47–61.

Rasmussen B, Bose P K, Sarkar S, Banerjee S, Fletcher I R and Mc Naughton N J 2002 1.6 Ga U–Pb zircon ages for the Chorhat Sandstone, Lower Vindhyan, India: possible implication for early evolution of animals; *Geology* **30** 103–106.

Ray J S, Martin M W and Veizer J 2002 U–Pb zircon dating and Sr isotope systematics of the Vindhyan Supergroup, India; *Geology* **30** 131–134.

Ray J S, Veizer J and Davis W J 2003 C, O, Sr and Pb isotope systematics of carbonate sequences of the Vindhyan Supergroup, India: age, diagenesis, correlation and implications for global events; *Precamb. Res.* **121** 103–140.

Sarangi S, Gopalan K and Kumar S 2004 Pb–Pb age of earliest megascopic eukaryotic alga bearing Rohtas Formation, Vindhyan Supergroup, India: Implications for Precambrian atmospheric oxygen evolution; *Precamb. Res.* **132** 107–121.

Sarkar S, Chakraborty P P and Bose P K 1996 Proterozoic Lakheri Limestone, central India: facies, paleogeography and physiography. In: Recent Advances in Vindhyan Geology (ed.) Bhattacharyya A, *Mem. Geol. Soc. Ind.* **36** 5–25.

Schidlowski M 2001 Carbon isotopes as biogeochemical recorders of life over 3.8 Ga of earth history: evolution of a concept. *Precamb. Res.* **106** 117–104.

Schieber J 1999 Microbial mats in terrigenous clastics: the challenge of identification in the rock record; *Palaios* **14** 3–12.

Sepkoski J J Jr 1982 Flat-pebble conglomerates, storm deposits and the Cambrian bottom fauna. In: Cyclic and Event Stratification (eds) G Einsele and A Seilacher (Berlin: Springer-Verlag), Pp. 371–385.

Shields G and Veizer J 2002 Precambrian marine isotope database: Version 1.1; *Geochem. Geophys. Geosys.* **3** U1–U12.

Singh I B 1973 Depositional environment of the Vindhyan sediments in the Son valley area; Recent Researches in Vindhyan, *Geology* **1** 140–152.

Snedden J W, Nummedal D and Amos A F 1988 Storm- and fair-weather combined flow on the central Texas continental shelf; *J. Sed. Pet.* **58** 580–595.

Tucker M E 1982 Storm-surge sandstones and the deposition of interbedded limestone: late Precambrian, southern Norway. In: Cyclic and Event Stratification (eds) G Einsele and A Seilacher (Berlin: Springer-Verlag), Pp. 363–370.

MS received 14 May 2004; accepted 13 September 2004